Radiation Physics and Chemistry 212 (2023) 111065

Contents lists available at ScienceDirect

Radiation Physics and Chemistry

journal homepage: www.elsevier.com/locate/radphyschem

Luminescence characteristics of white light emitting $BaGa_2O_4:Dy^{3+}$ phosphors for LEDs and stress sensing applications

M.S. Anju [a], N. Gopakumar [a,*], P.S. Anjana [b], M.R. Revupriya [a]

[a] Department of Physics, Mahatma Gandhi College, University of Kerala, Thiruvananthapuram, 695004, India

[b] Department of Physics, All Saints' College, University of Kerala, Thiruvananthapuram, 695007, India

ARTICLE INFO

Handling Editor: Dr. Chris Chantler

Keywords:
Photoluminescence
Thermoluminescence
Mechanoluminescence
Gallates
Phosphors

ABSTRACT

A series of single-phase white-light-emitting $BaGa_2O_4:xDy^{3+}$(x = 0.1,0.3,0.5,0.7,1) phosphors have been synthesised using solid-state reaction technique. The structural studies using the X-ray diffraction (XRD) technique indicate that the phosphors are single-phase and Scanning Electron Microscope (SEM) study reveals that the particle size is in micrometer range. The phosphors emit white light with peaks at 346 nm, 357 nm, 386 nm, and 426 nm generated by Dy^{3+} ion transitions ($^6H_{15/2} \rightarrow {}^6P_{7/2}$), ($^6H_{15/2} \rightarrow {}^6P_{9/2}$), ($^6H_{15/2} \rightarrow {}^4F_{7/2}+{}^4I_{13/2}$) and ($^6H_{15/2} \rightarrow {}^4G_{11/2}$). The colour coordinates calculated for $BaGa_2O_4:xDy^{3+}$ (x = 0.5,0.7) phosphors are identical to the conventional white light. $BaGa_2O_4:Dy^{3+}$ exhibits good Mechanoluminescence (ML) response at varied impact velocities for both unirradiated and gamma-irradiated samples. This characteristic is reasonably beneficial in the development of damage and pressure sensors. Thermoluminescence (TL) analysis shows a single glow curve of similar shape irrespective of increasing irradiation, and the TL parameters have been calculated.

1. Introduction

Gallium oxide (Ga_2O_3) is an emerging ultrawide bandgap (UWBG) semiconducting material that may be exploited in a variety of applications, including opto electronics, power electronics, solar blind photodetectors, and deep ultraviolet optoelectronics (Xuanhu et al., 2021). Its high band gap makes it possible to alter its luminescence by adding the proper ions to the Ga_2O_3 lattice. Doping of optically activated rare earth (RE) ions in Ga_2O_3 enables the development of devices that emit light in the ultraviolet and visible range (Zhao et al., 2011).

Gallium oxide is a wide band gap (4.9 eV) material with great mechanical strength, UV transparency, thermal and chemical stability, and is a promising material for optoelectronic devices (Wei et al., 2013). Since both RE and Ga^{3+} ions have the same electro negativity and atomic size, it is assumed that Dy^{3+} ions will be able to replace Ga^{3+} ions at the eight tetrahedral and sixteen octahedral positions in $BaGa_2O_4$ doped Dy^{3+} phosphors. S. H. M. Poort et al. reported the structure of barium aluminates and gallates. There are two distinct barium sites in $BaGa_2O_4$, one of which occurs three times more frequently than the other. On both sites, the nine oxygen ions are coordinated. $BaGa_2O_4$ is isostructural with $BaAl_2O_4$; hence the structure of $BaGa_2O_4$ is that of a stuffed tridymite (Poort et al., 1995). $BaGa_2O_4$ has received a lot of attention as a phosphor material for LEDs. Previous research has shown that the rare earth-free $BaGa_2O_4$ luminescent compound emits in the bluish region (Noto et al., 2017). Halyana Klym reported the evolution of free volumes in polycrystalline $BaGa_2O_4$ ceramics by doping with Eu^{3+} ion (Klym et al., 2021).

Rare earth doped phosphors emit bright light, have a longer lifetime, and have outstanding optical properties due to their chemical and thermal stability, high luminescence, and colour purity (Liu et al., 2019). Hojin Ryu and Hee Dong Park investigated the photoluminescent properties of zinc gallate doped with various rare earths and found that doped zinc gallates have higher emission intensity than undoped zinc gallate (Ryu and Park, 1997). The Dy^{3+} ion is an ideal choice for studying emissions in the visible and mid-infrared domains, which are needed in a variety of applications such as technical, military, telecommunications, displays, medical, and so on. This is widely known from published data that active Dy^{3+} ion has two strong luminescence bands in the visible range, blue at 490 nm ($^4F_{9/2} \rightarrow {}^6H_{15/2}$) and yellow at 590 nm ($^4F_{9/2} \rightarrow {}^6H_{13/2}$). White light is created when these lights are mixed, and this has been used in solid state lighting technologies in recent years (Vijayakumar et al., 2018)

White light emitting diodes (LEDs) have gained more and more attention recently due to their numerous benefits (Qiao et al., 2019).

* Corresponding author.
E-mail address: gopkumar.n@gmail.com (N. Gopakumar).

https://doi.org/10.1016/j.radphyschem.2023.111065
Received 23 November 2022; Received in revised form 24 May 2023; Accepted 28 May 2023
Available online 7 June 2023

White LEDs are regarded as the fourth generation of light sources since they are more efficient, brighter, durable, and environmentally friendly than older light sources (Chao Li et al., 2018; Xiong et al., 2018; Zhao et al.,2019). The most popular technique for creating white LEDs is to mix a yellow phosphor called YAG:Ce^{3+} with a blue LED chip called GaN. Due to the absence of a red component, this type of white LED has a number of disadvantages, including a low colour rendering index and a high correlated colour temperature (Xiong et al., 2018; Zhao et al., 2019). White LEDs should exhibit unique optical performance in various application circumstances since they can be employed not only in the lighting industry but also in the display and medical fields (Hu et al., 2019; Zhao et al.,2018; Chen et al 2019). S.Chemingui reported the white light generation and luminescence characteristics of Dy^{3+}doped $KLa(PO_3)_4$ (Chemingui et al., 2015). R.Vijayakumar reported the colortunable properties of Dy^{3+} and Eu^{3+}co-doped $Na_3Sc_2(PO_4)3$ phosphors (Vijayakumar et al., 2018). R.Cao recently reported the luminescence properties of rare earth doped silicate phosphors for LED application (Cao et al., 2022a; 2022b). Though many papers have been published in Dy^{3+} phosphors, very little publication on gallium oxide phosphors doped with Dy^{3+} has taken place to date.

Mechanoluminescence (ML)-based stress sensing has received much interest because of its properties of remoteness and having a equitable response to mechanical stimuli as well as its great potential for stretchability, biocompatibility and self-powering. Significant advancements have been made in the design of devices, study of applications, and discovery of ML materials over the last few decades. ML-based sensing has significant potential for future improved stress sensing application (Zhuang and Xie, 2021). Local mechanical stimulus in solid phosphors can be converted to light emission, a process known as mechanoluminescence. Some phosphors, such as $ZnGa_2O_4$:Mn and $MgGa_2O_4$:Mn, have been discovered to produce visible light under mechanical stress, a phenomenon known as mechanoluminescence (ML), as reported by H. Matsui (Matsui et al., 2000). Mechanical stimulus in solids includes impact, compression and friction (Zhang et al., 2013). ML sensors are gaining interest due to their applications in areas such as safety monitoring, crack detection in bridges and tunnels, and identification of personal handwriting using dynamic pressure mapping. Due to the high intensity irradiation of light required for ML emission in alkali halide ML materials, such applications are limited (Fu et al., 2018). There has been no report on the ML from $BaGa_2O_4$:Dy^{3+} till date.

When a solid is exposed to ionising radiations, some or all of the incident beam's energy is absorbed. Electrons and holes are generated, and they migrate and become trapped at the defect locations in the phosphor material. When irradiated phosphor is heated, electrons and holes escape from their respective trapped sites and recombine with their counter parts, resulting in annihilation in the form of phosphorescence. The glow curve of phosphors is a thermoluminescence intensity vs temperature plot with single or many peaks (Manam et al., 2010; Li et al., 2018; Sharma et al., 2010). The glow curve provides the TL parameters such as activation enery (E), frequency factor (s) and order of kinetics (b) (Hunter et al., 2012). L.L.Noto reported the structure and thermoluminescence properties of composite $ZnTa_2O_6$/$ZnGa_2O_4$ compound doped with Pr^{3+} (Noto et al., 2014). The luminescence dynamics of $MgGa_2O_4$ produced via solution combustion synthesis and states that the thermoluminescence spectroscopy associated $MgGa_2O_4$ are of general order of kinetics (Mlotswa et al., 2020). The preliminary thermoluminescence of $BaGa_2O_4$ is reported by L.L.Noto and concluded that the kinetics involved are neither first nor second order (Noto et al., 2017). $BaGa_2O_4$ is a suitable host lattice for doping trivalent lanthanide series for the preparation of promising luminous materials. However, no major photoluminescence (PL), thermoluminescence (TL), or mechanoluminescence (ML) research with rare earth doped $BaGa_2O_4$ has been published to date. Hence the present study describes the preparation of dysprosium doped barium gallate phosphor using a typical solid state reaction approach, as well as the investigation of its photoluminescence (PL), mechanoluminescence (ML), and thermoluminescence (TL) properties.

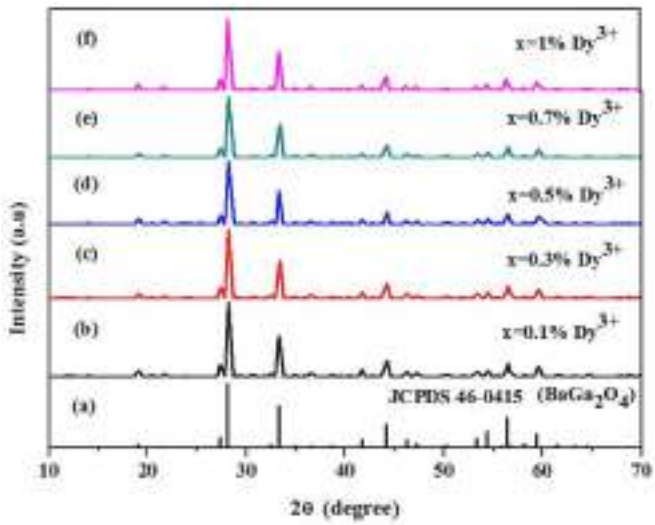

Fig. 1. Powder X-ray diffraction patterns of $BaGa_2O_4$:xDy^{3+} (x = 0.1,0.3,0.5,0.7,1) phosphors.

2. Experimental

The $BaGaO_4$:xDy^{3+}(x = 0,0.1,0.3,0.5,0.7,1) phosphors were prepared by traditional solid state reaction method. High purity $BaCO_3$(99.99%), Ga_2O_3(99.99%) and Eu_2O_3(99.99%) (Sigma Aldrich) were used as the starting reagents. x= (0,0.1,0.3,0.5,0.7,1) % of Dy^{3+} is replacing the Ga atom in $BaGaO_4$:xDy^{3+} phosphor. The ionic radii of Ba^{2+} (1.38 nm), Ga^{3+} (0.062 nm) and Dy^{3+} (0.092 nm) show that Dy^{3+} ions replace the Ga^{3+} site without interfering with the $BaGa_2O_4$ phase. The reagents were completely mixed for 2 h using an agate motor and pestle in double distilled water (mixing medium). The resulting slurry was then dried in a hot air oven, calcined for 5 h at 1200 °C and then ground well for 2 h. The structural analysis of the samples were done using X-ray diffractometer (XRD) [Model D8 Advance AntonnPaar, TTK450 using Cu X-ray source (λ = 1.5406 Å)]. The surface morphology of the phosphor was studied using a Hitachi SEM S-4300 Scanning Electron Microscope.D8Advance]. The XPS (X-ray Photoelectron Spectroscopy) analysis of the $BaGa_2O_4$:0.7Dy^{3+} sample was taken using the Thermo Scientific ESCALAB Xi + XPS system. The absorption study was

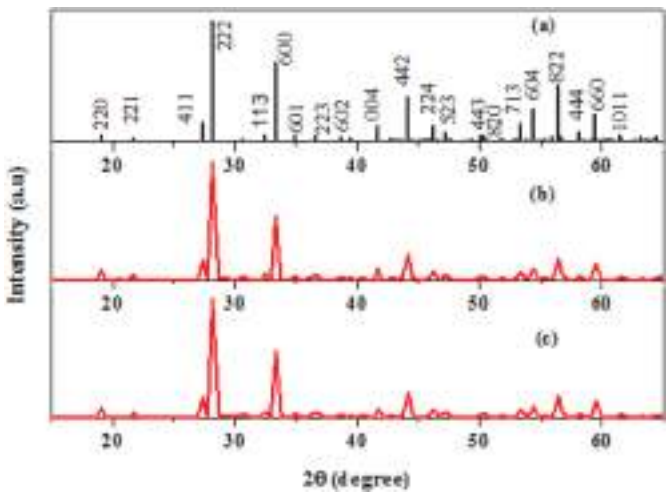

Fig. 2. (a) JCPDS of $BaGa_2O_4$(46–0415), (b) X-Ray diffraction pattern of prepared $BaGa_2O_4$, (c) X-ray diffraction pattern of $BaGa_2O_4$:1% Dy^{3+} phosphor.

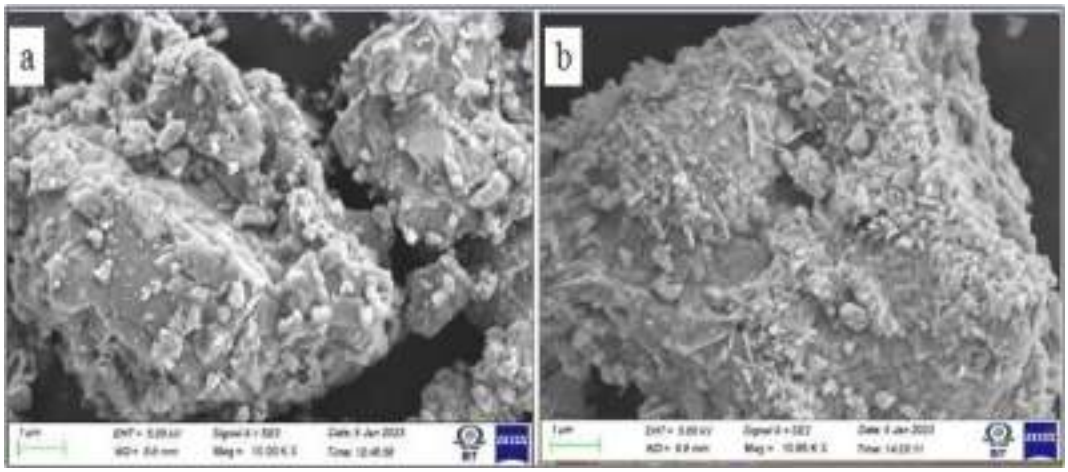

Fig. 3. FE-SEM micrographs of a. Pure $BaGa_2O_4$ and b. $BaGa_2O_4$:0.7Dy^{3+} phosphors.

carried out in the range 200–800 nm using PerkinElmer LAMBDA 365 UV–Visible spectrometer. Photoluminescence was recorded using Horiba Fluorolog fluorescence spectrometer with TCSP (Model Fluorolog3 TCSPC)). Thermoluminescence study of gamma irradiated phosphor was conducted using Nucleonix TL/OSL Research reader (modelTL1008). The Mechanoluminescence studies of phosphor powders were conducted by impact method using indegenously developed ML measuring apparatus. A photomultiplier tube (PMT 931A) is positioned below the Lucite plate and connected to a digital storage oscilloscope (Tektronix TSB 1102B). When a of mass 100 g strikes the phosphor sample, ML has been generated.

3. Results and discussion

3.1. X-ray diffraction analysis

Fig. 1 shows the XRD patterns of $BaGa_2O_4$:xDy^{3+} (x = 0.1,0.3,0.5,0.7,1) phosphors. The XRD patterns of $BaGa_2O_4$ and $BaGa_2O_4$:Dy^{3+} samples compared with the standard ICDD data are shown in Fig. 2. All the peaks of the prepared samples are indexed and are in good agreement with ICDD card no 46–0415 of $BaGa_2O_4$. The XRD patterns of all the samples are identical, with no extra peak corresponding to the impurity phase, indicating that the samples are single phase with same crystal structure. It denotes that the synthesised phosphor has hexagonal structure with a space group of $P6_3$ (Acuna et al., 2017). The sharp peaks seen in the XRD patterns of the samples, suggest good crystallinity (Liu et al., 2012; Yu et al., 2018). Figs. 1 and 2, clearly show that doping Dy^{3+} in $BaGa_2O_4$ has no effect on the crystal structure of the samples. The intensity of the peaks, however, decreases with increasing doping concentration while their peak positions remain unchanged. With the addition of 1mol percent Dy^{3+}, some extra peaks corresponding to impurity appear. This demonstrates that the maximum doping concentration for this series is less than 1mol percent Dy^{3+} in $BaGa_2O_4$.

3.2. Morphology

The FE-SEM images of pure $BaGa_2O_4$ and $BaGa_2O_4$:0.7Dy^{3+} are shown in Fig. 3. Doping Dy^{3+} ions into the host lattice does not induce a significant change in the crystal morphology but rod shaped grains of 200–500 nm range can see in the doped phosphor, this may be due to the presence of dysprosium oxide. Agglomeration is observed due to high temperature solid state reaction. Samples prepared by high temperature reactions exhibit agglomeration, which is the reaction's signature (Fu et al., 2018; Manam and Das, 2010). The nature of agglomeration in doped sample is seen to be less than that of pure. The FE-SEM image

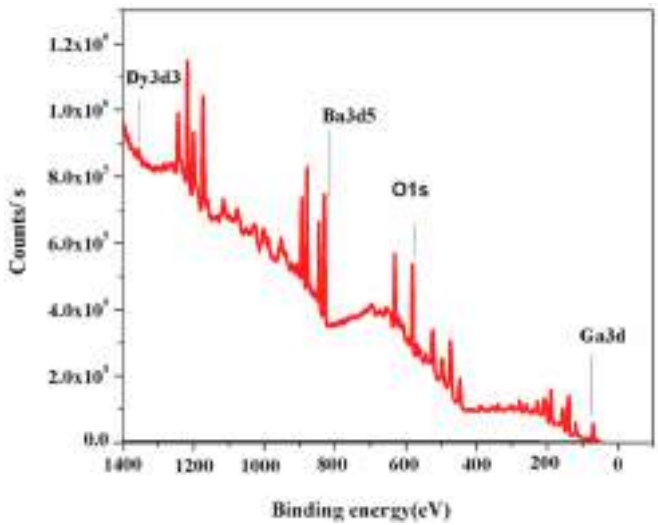

Fig. 4. X-ray photoelectron spectroscopy of $BaGa_2O_4$:0.7Dy^{3+} phosphor.

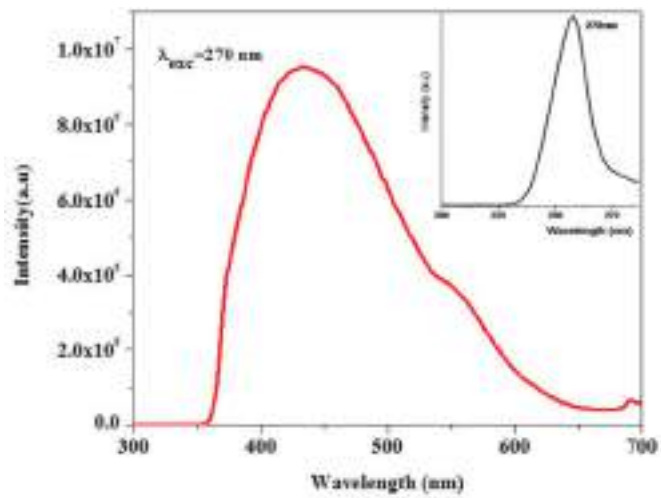

Fig. 5. PL emission spectra of $BaGa_2O_4$ excited at 270 nm, inset shows the excitation spectrum.

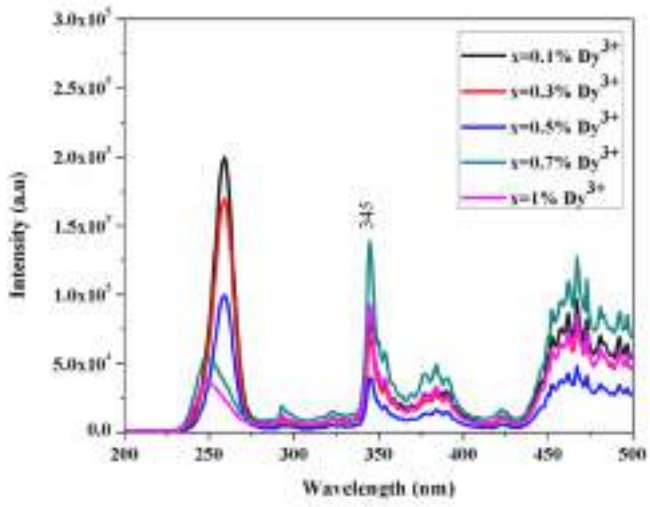

Fig. 6. Excitation spectra of.$BaGa_2O_4$:xDy^{3+} (x = 0.1,0.3,0.5,0.7,1) phosphors.

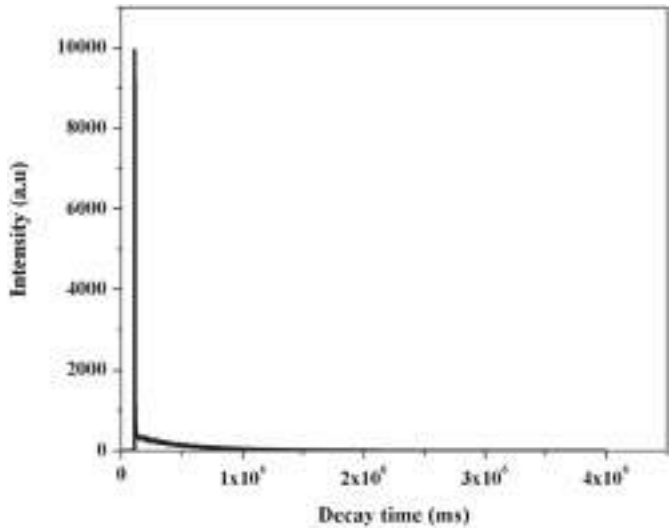

Fig. 8. Decay curve of $BaGa_2O_4$:0.7Dy^{3+} Phosphor.

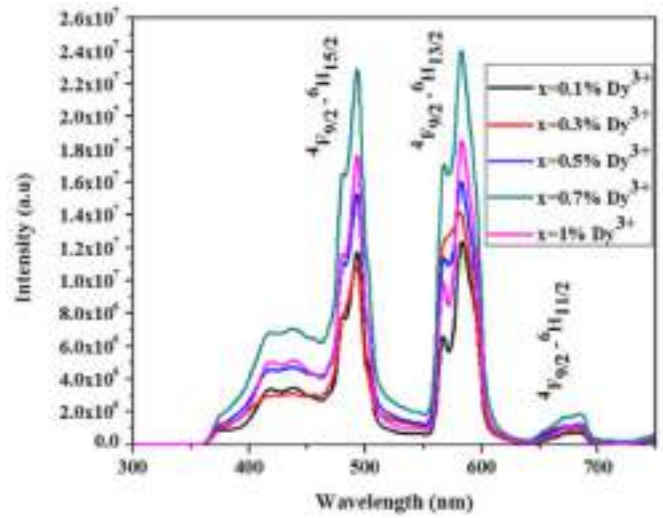

Fig. 7. Emission spectra of $BaGa_2O_4$:x Dy^{3+} phosphors excited at 345 nm.

clearly shows that the particle size of the prepared sample ranges in 1–3 μm range.

3.3. XPS analysis

Fig. 4 shows the X-ray photon spectroscopy of $BaGa_2O_4$:0.7Dy^{3+} phosphor in the range 0–1400 eV. The occurrence of Dy^{3+} is identified by the Wide scan XPS spectra of $BaGa_2O_4$:0.7Dy^{3+}. In the XPS spectra, the presence of the elements Barium (Ba3d5, 785eV), Gallium (Ga3d, 25eV) and Oxygen (O1s, 535eV) was detected. The peaks detected at 1335 eV is due to the presence of Dy^{3+} (Dy3d3) in the sample.

3.4. Photoluminescence studies

$BaGa_2O_4$ shows emission in the bluish region when excited at 270 nm and is shown in Fig. 5 (Liu et al., 2019). The PL emission spectrum of $BaGa_2O_4$ has a broad emission range from 350 to 650 nm, as seen in Fig. 5 the inset shows the excitation spectrum. The photoluminescence excitation spectra of $BaGa_2O_4$:xDy^{3+} sample for an emission at 580 nm is shown in Fig. 6. The excitation spectra consist of a broad band from 230 nm to 280 nm, and are perhaps caused by the absorption of host. The region of host absorption for various Dy^{3+} concentrations clearly varies (Gao and Li, 2018). The sharp peaks beyond 350 nm indicate the f-f transition of Dy^{3+} at 345 nm ($^6H_{15/2} \rightarrow {}^6P_{7/2}$), 357 nm ($^6H_{15/2} \rightarrow {}^6P_{9/2}$), 386 nm ($^6H_{15/2} \rightarrow {}^4F_{7/2}+{}^4I_{13/2}$) and 426 nm ($^6H_{15/2} \rightarrow {}^4G_{11/2}$) 448 nm ($^6H_{15/2}$-$^4I_{15/2}$) and 480 nm ($^6H_{15/2}$-$^4F_{9/2}$) (Chemingui et al., 2015). With increasing concentrations of dysprosium, the intensity of absorption peaks of the intra-configurational 4f transitions of Dy^{3+} increase (Yu et al.,2018; Lee et al., 2009; Tangoulis et al., 2018)

A spectral shift towards higher wavelengths (i.e. lower energy and lower frequency) is called a red-shift. The location of host absorption (225–275 nm) changes when the Dy^{3+} concentration increases to 0.7 and1% due to red shift. The excitation intensity observed to be higher for 0.7% Dy^{3+} concentration and then decreases (Sun et al., 2010). Multiple lines observed in the excitation spectra indicate transitions involving dopants. The excitation spectrum includes a series of linear peaks located between 375 and 500 nm attributed to the electronic transitions of Dy^{3+} ion,$^6H_{15/2}$-$^6P_{5/2}$ (364 nm), $^6H_{15/2}$-$^4K_{17/2}$ (386),$^6H_{15/2}$-$^4I_{15/2}$ (448 nm) and $^6H_{15/2}$-$^4F_{9/2}$ (480 nm) (Chemingui et al., 2015). The presence of multiple transitions of Dy^{3+} may cause the emission peak unsmooth in 375–500 nm range.

Fig. 7 shows the emission spectra of the phosphor when excited at 345 nm. There is a wide band appearing between 400 and 460 nm, which is most likely due to the emission from $BaGa_2O_4$. The magnetic dipole transition of $^4F_{9/2} \rightarrow {}^6H_{15/2}$ and the forced electric dipole transition of $^4F_{9/2} \rightarrow {}^6H_{13/2}$ are attributed to two strong peaks in the visible areas of the phosphors at 490 nm and 590 nm, respectively. There is also a weak red emission at 670 nm due to the $^4F_{9/2} \rightarrow {}^4H_{11/2}$ transition. For blue, yellow, and red emission, these peaks are attributed to energy transitions from the excited state $^4F_{9/2}$ to three distinct ground states $^6H_{15/2}$, $^6H_{13/2}$, and $^6H_{11/2}$ (Gao and Li, 2018; Tangoulis et al., 2018).The intensity of emission peak enhances with increasing Dy^{3+} concentration and reaches maximum at 0.7% and it starts to decrease further with the increasing concentration. When the doping concentration reaches the optimum value, concentration quenching occurs and this gradually decreases the luminescence intensity. When the distance between activator ions diminishes, excitation energy migrates non-radiatively among these dysprosium ions, resulting in concentration quenching (Jamalaiah et al., 2019; Praveena et al., 2016).

3.5. Decay characteristics

The decay curve of $BaGa_2O_4$:0.7Dy^{3+} is shown in Fig. 8. The decay curve shows a sharp rise followed by a single exponential decay. Decay times can be calculated by curve fitting method based on the exponential function $I = A(\exp(-t/\tau_1)-\exp(-t/\tau_2))$, where I is the luminescence

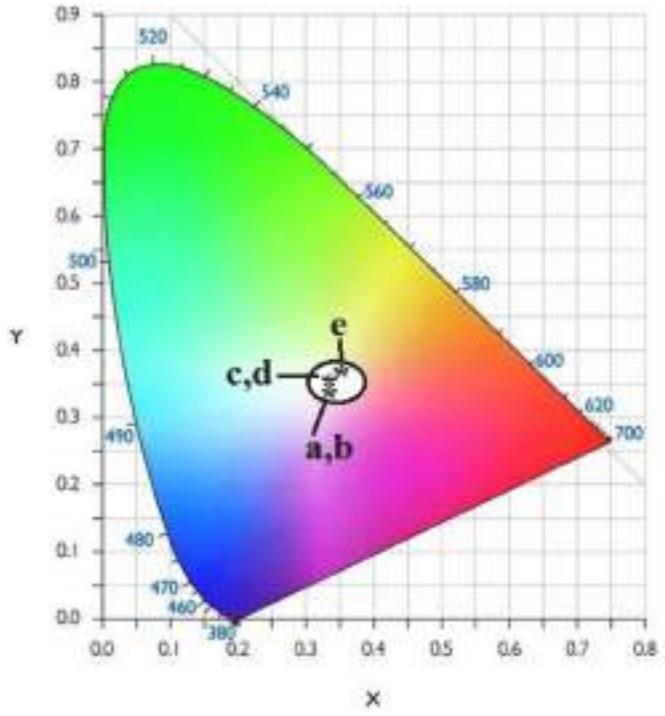

Fig. 9. Chromatic diagram of $BaGa_2O_4$:xDy^{3+}(x = 0.1,0.3,0.5,0.7,1) phosphor excited at 345 nm.

Table 1
CIE and CCT values of $BaGa_2O_4$:xDy^{3+}phosphors.

Phosphors prepared	CIE Cordinates	CCT(K)
Excitation:345 nm		
$BaGa_2O_4$:0.1Dy^{3+}	x = 0.33 y = 0.32	5620
$BaGa_2O_4$:0.3 Dy^{3+}	x = 0.33 y = 0.32	5620
$BaGa_2O_4$:0.5 Dy^{3+}	x = 0.33 y = 0.33	5613
$BaGa_2O_4$:0.7 Dy^{3+}	x = 0.33 y = 0.33	5613
$BaGa_2O_4$:1 Dy^{3+}	x = 0.35 y = 0.36	4846

intensity; A is a constant; t is the time; τ_1 and τ_2 are decay time and rise time. The emission band of 590 nm has life times of 1.083 and 1.071 ms for 345 nm excitation.

3.6. Chromaticity coordinates

Fig. 9 shows the chromaticity diagram of $BaGa_2O_4$:xDy^{3+}(x = 0.1,0.3,0.5,0.7,1) mol% phosphors excited at 345 nm. All the points pass through the green region of the CIE diagram. Table 1 shows the CIE and CCT values of $BaGa_2O_4$:xDy^{3+} phosphors. It is found that the CIE co-ordinates are a = (0.33,0.32), b = (0.33,0.32) c = (0.33,0.33), d = (0.33,0.33), and e = (0.35,0.36) for $BaGa_2O_4$:xDy^{3+} (x = 0.1,0.3,0.5,0.7,1) phosphors respectively. The colour coordinates summarized in the table reveals that $BaGa_2O_4$phosphor doped with 0.5 and 0.7 mol% Dy^{3+} show pure white colour emission. All the colour co-ordinates are closer to the standard D65 day light with c-ordinates of (0.32,0.33) (Praveena et al., 2016; McCamy, 1992). The colour co-ordinates of all of the phosphors investigated are extremely near to the normal white light (0.33, 0.33). Since the emission spectra of the synthesised $BaGa_2O_4$:xDy^{3+} (x = 0.1,0.3,0.5,0.7,1) phosphors cover the entire visible wave length range of 380–700 nm, the quality of white light produced may be excellent, with an outstanding colour rendering index.

Table .1 shows the CIE coordinates and corresponding CCT (correlated colour temperature) values. The CCT value is determined using the McCamy Method (McCamy et al., 1992).

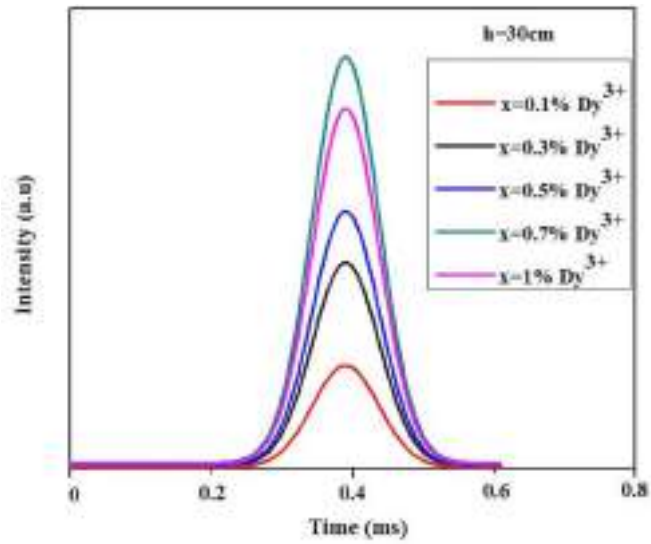

Fig. 10. Variation of ML intensity with time of $BaGa_2O_4$:xDy^{3+}(x = 0.1,0.3,0.5,0.7,1) phosphors.

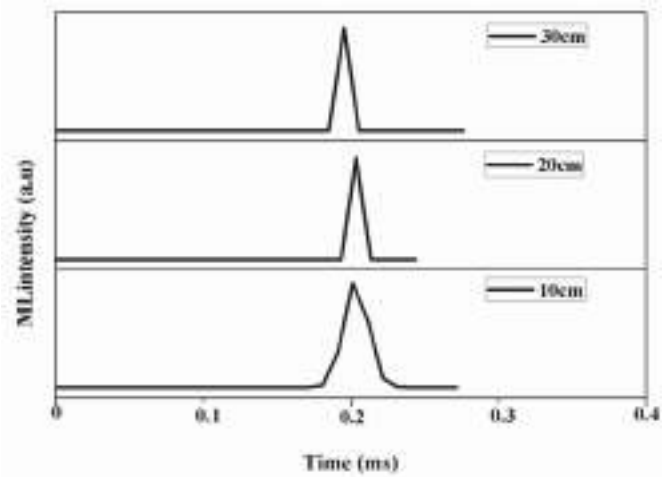

Fig. 11. Dependence of ML intensity of $BaGa_2O_4$:$0.7Dy^{3+}$ for different impact velocities.

$$CCT = -449n^3 + 3525n^2 - 6823.3n + 5520.33 \quad (1)$$

where n = $(x-x_e)/(y-y_e)$, the chromaticity coordinates are (x, y), and the (x_e, y_e) coordinates are (0.3320, 0.1858), these correspond to the epicentre of convergence of the CIE 1931 chromaticity diagram's isotemperature lines.

The CCT of all phosphor samples are greater than 5000K, except for x = 1 mol% percent (4846K). CCT less than 5000K is used as the warm white light for home appliances and more than 5000K for cold white light in business lighting applications (Tangoulis et al., 2018; Sun et al., 2010). The values CCT decreases with increase in Dy^{3+} concentration.

3.7. Mechanoluminescence

Mechanoluminescence (ML) is the light emitted by a material as a result of deformation or fracture produced by stress. The ML measuring equipment used the impact method to record the ML readings. The ML response is monitored with change in impact velocity. A 100g load is dropped from heights of 10 cm, 20 cm, 30 cm. The impact velocity is determined using the formula $\sqrt{2gh}$, where g is the acceleration due to

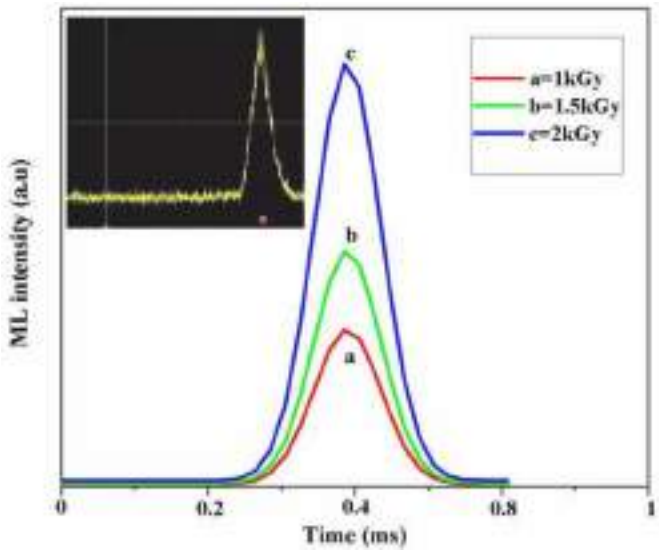

Fig. 12. ML spectra of $BaGa_2O_4$:0.7Dy^{3+} phosphor at10 cm height for various gamma ray dosages, inset shows the recorded ML spectra.

gravity and h is the height from which the weight is falling. When the load strikes the sample, light emission occurs, which is monitored with a Photo Multiplier Tube. Fig. 10 shows the ML spectra of $BaGa_2O_4$:xDy^{3+} (x = 0.1,0.3,0.5,0.7,1) phosphor detected from a height of 30 cm. Single emission peak is observed as a result of charge transfer mechanism during mechanical process. It is observed that the intensity of ML glow curve increases with increase in doping concentration of Dy^{3+} up to 0.7 mol%, and then decreases for higher concentrations due to concentration quenching. An approximate linearity of emission intensity against applied load is observed, indicates that the sample can be used as sensors to detect stress (Pateria et al., 2015).

The ML glow curves of $BaGa_2O_4$:0.7Dy^{3+} with varied impact velocities are shown in Fig. 11. It is worth noting that the phosphor without irradiation has a very good ML response. For varied impact velocities (10 cm,20 cm,30 cm), the intensity of the ML peak increases and reaches a maximum at a height of 30 cm. The existence of electron and hole traps in the samples causes the ML intensity to decline beyond this (30 cm) impact velocity. The ML intensity cannot be fully recovered when the damaged sample is treated with gamma irradiation. Researchers have offered a number of explanations to explain the origins of ML. When the load makes an impact on the sample, the surface of local piezoelectric regions gets positively charged and the other surface becomes negatively charged. The trap-depth reduces due to induced piezoelectric field and that causes detrapping of electrons. This detrapped electrons move to the conduction band. Some of the electrons move to the conduction band may get accelerate and subsequently excite dysprosium ions. Thus the de-excitation of dysprosium ions gives rise to the light emission (Fu et al., 2018; Kher et al., 2006; Shrivastava and Kaur, 2015)

It is observed that as height increases, the peak ML intensity swings towards shorter time with height which is due to the increase in impact velocities. It can be observed that the ML intensity increases with time, reaches a maximum, and then drops. Mechanical energy is turned into photon energy when phosphor powder is fractured by the impact of a load. The light produced is mostly caused by a rise in pressure or an increase in the height of the load (Kher et al., 2006; Shrivastava and Kaur, 2015).

Fig. 12 shows the ML spectra sample recorded by dropping at a height of10cm, irradiated under 1 kGy, 1.5 kGy and 2 kGy.Very strong ML emission intensity from irradiated phosphor has been detected at low impact velocities. The instrument cannot read any higher impact velocities than 10 cm height because the emission intensities are beyond the oscilloscope's attenuation limit. The intensity of gamma irradiated

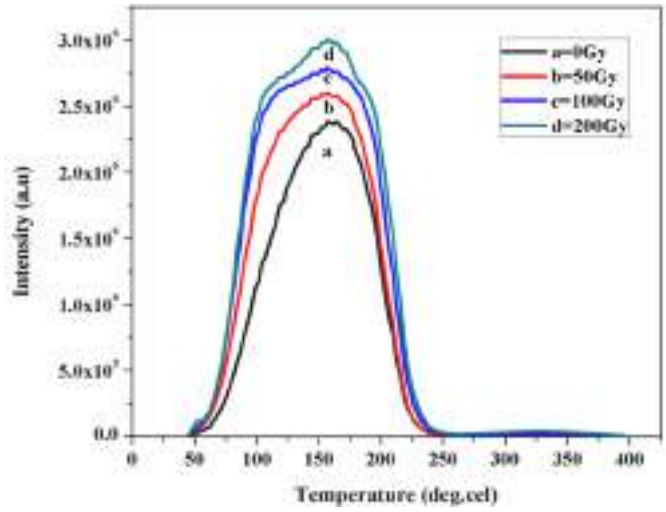

Fig. 13. TL Glow curve of $BaGa_2O_4$:0.7 Dy^{3+} phosphor for various gamma dosages.

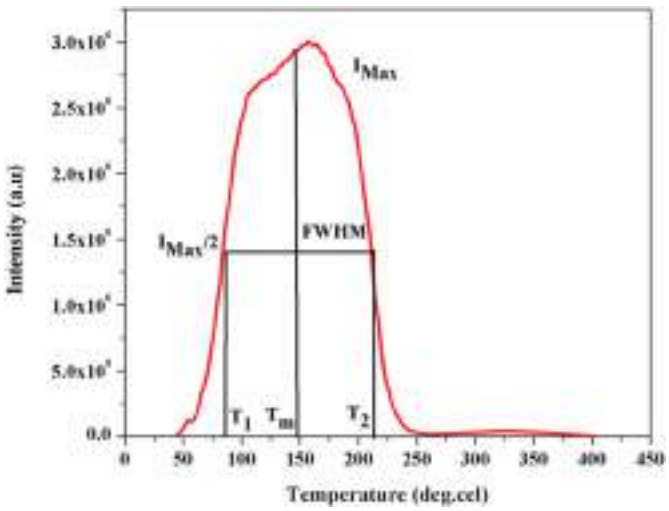

Fig. 14. The TL glow curve of $BaGa_2O_4$:0.7Dy^{3+} phosphor showing various parameters.

samples is measured to be much higher than that of unirradiated samples. When gamma-irradiated phosphor is fractured, a strong electric field is generated owing to the charging of freshly created surfaces near the crack tip. Bands may bend as a result of the electric field. The holes are released from the hole trap by bending the conduction band, valence band, and trapping. As a result, energy may be released by the recombination of holes moving in the valence band with electron trapping sites.De-excitation of an excited Dy^{3+} ion may result in Dy^{3+} ion luminescence. The presence of a single peak in the ML spectrum indicates that the defect centres responsible for ML emission are activated almost simultaneously as a result of the load's effect (Shrivastava et al., 2015)

The increase in ML intensity with gamma-irradiation suggests that the ML of $BaGa_2O_4$:Dy^{3+} is not due to charge carrier recombination caused by dielectric breakdown during fracture (Shrivastava et al., 2015; Lakshmanan et al., 2008).

3.8. *Thermoluminescence of $BaGa_2O_4$:0.7 Dy^{3+} phosphor*

The TL glow curve of 50–300 Gy gamma irradiated $BaGa_2O_4$:0.7 Dy^{3+} at a heating rate of 2 °C/s is shown in Fig. 13. The glow curve shows a single peak of similar shape for varying gamma irradiation

Table 2
TL parameters of $BaGa_2O_4$:0.7Dy^{3+}.

Dose (Gy)	Heating rate	T_1 (°C)	T_2 (°C)	T_m (°C)	(T_2-T_1) (°C)	T_2-T_m (°C)	$\mu_g = \frac{\delta}{\omega}$	Activation energy (eV)	Frequency factor(S^{-1})
300	2 °C/s	80	215	147	135	68	0.50	0.38	$5.23*10^{12}$

dosages. The TL intensity increases with increasing dose and no shifts in the peaks position have been observed. The increase in the relative intensity of the peaks has been linked to a change in the number of luminescent/trapping centres. The illumination peaks at lower temperatures (147 °C) show that the phosphor is a promising material for display technology (Premkumar et al., 2013; Pathak and Kurchania, 2016).

The material's utility for ionising radiation dosimetry is confirmed by the existence of a high temperature peak (Pathak and Kurchania, 2016). The trapping parameters such as order of kinetics, activation energy, and frequency factor are determined to understand the properties of the synthesised phosphor. The glow curve of 0.7Dy^{3+} doped $BaGa_2O_4$ phosphor irradiated with 300 Gy is shown in Fig. 14 for determining the various parameters.

3.8.1. Order of kinetics

The order of kinetics of the glow curve is determined by calculating the symmetry factor,

$$\mu_g = \frac{\delta}{\omega} = (T_2 - T_m) \Big/ (T_2 - T_1) \quad (2)$$

Where $\omega = T_2$-T_1 is total half intensity width also FWHM. $\delta = T_2$-T_m, is high temperature half width. The symmetric factor of the glow curve peaking at 147 is found to be 0.50, which suggests that the peak obeys second kinetics.

3.8.2. Activation energy (E)

Activation energy (E) is calculated by using Chen's equation

$$E = c_\gamma \left[\frac{kT_m^2}{\gamma}\right] - b_\gamma [2kT_m] \quad (3)$$

Where, T_m is the glow peak temperature, c_γ and b_γ are constants for second order kinetics and values of these constants are 1.71 and 0 respectively. γ is the high temperature half width (δ) and k is the Boltzmann's constant. The activation energy of the sample peaking at 147 °C is found to be 0.38 eV.

3.8.3. Frequency factor

The information regarding the probability to escape of electrons from their traps after the exposure of ionising radiation is obtained from frequency factor. Frequency factor is strongly depending on temperature; history of exposure information up to a certain period of time can also be related with it (Pathak and Kurchania, 2016; Aitasalo et al., 2004).

The frequency factor is calculated by the following equation

$$\beta E \Big/ kT_m^2 = s[1 + (b-1)2kT_m / E] exp[-E / kTm] \quad (4)$$

Here β is the heating rate. Frequency factor of the prepared sample is found to be 5.23×10^{12} s^{-1}. Frequency factor depends on various factors like number of traps and corresponding trap depth following the irradiation, excitation dose, radiation type and energy (Pathak and Kurchania, 2015; Ahmed et al., 2016). **The kinetic parameters of TL glow peak of $BaGa_2O_4$:0.7 Dy^{3+} is displayed in** Table 2.

4. Conclusions

Single-phased $BaGa_2O_4$:xDy^{3+}(x = 0.1,0.3,0.5,0.7,1) phosphors have been successfully synthesised by solid-state reaction technique. When stimulated at 345 nm, the emission spectra of all the phosphors show a broad band between 400 and 460 nm, two peaks at 490–590 nm, and a weak red emission at 670 nm. These peaks are attributed to energy transitions from the excited state $^4F_{9/2}$ to three different ground states $^6H_{15/2}$, $^6H_{13/2}$, and $^6H_{11/2}$ for blue, yellow, and red emission. The colour coordinates obtained for $BaGa_2O_4$:xDy^{3+} phosphors are close to normal white light, as defined by CIE 1931, which specifies the white LED application of synthesised phosphor. The ML spectrum has been recorded with increasing impact velocities. With higher impact velocities, the emission intensity rises. Irradiated samples have a higher ML intensity than unirradiated ones. The total ML intensity is found to be increasing linearly for both unirradiated and gamma irradiated samples. The approximate linearity of emission intensity against applied load indicates that the phosphor material can be utilised as stress sensors. The TL intensity of the $BaGa_2O_4$:0.7Dy^{3+} phosphor increases with dosage of gamma-ray. The phosphor material's ability to illuminate at lower temperature (147 °C) indicates that it could be useful for radiation dosimetry. Based on the findings, the synthesised $BaGa_2O_4$:xDy^{3+} phosphor appears to be promising for various luminous applications.

Declaration of competing interest

The authors declare that they have no known competing financial interests or personal relationships that could have appeared to influence the work reported in this paper.

Data availability

Data will be made available on request.

Acknowledgments

The authors are thankful to Sophisticated Testing & Instrumentation Centre (STIC), Cochin Universityfor providing facility for XRD characterization and SEM analysis. We are also grateful to Sophisticated Analytical Instruments Facility (SAIF), Department of Environmental science, M.G University for providing facility for PL analysis. The authors are thankful to Dr.Panigrahi, IGCAR, Chennai for TL analysis.

References

Acuna, W., Tellez, J.F., Macias, M.A., Sandrine, P.R., Gauthier, G.H., 2017. Synthesis and characterization of $Baga_2O_4$ and $Ba_3Co_2O_6(CO_3)_{0.6}$ compounds in the search of alternative materials for Proton Ceramic Fuel Cell (PCFC). Solid State Sci. 24, 61–68.

Ahmed, K., Dahane, K., Khaidukov, N.M., Alves, N., 2016. Study of thermoluminescence mechanisms in $LaAlO_3$:Ce,Dy crystals. Optik 127, 6009–6014.

Aitasalo, T., Holsa, J., Jungner, H., Lastusaari, M., Niittykoski, J., Parkkine, M., Valtonen, R., 2004. Eu^{2+} doped calcium aluminates prepared by alternative low temperature routes. Opt. Mater. 26, 113–116.

Cao, R., Jiang, Z., Chen, T., Liang, H., Yi, X., Zhong, Y., Zhang, H., Luo, W., 2022a. Study on the luminescence properties and energy transfer of $Na_4CaSi_3O_9$:Ce^{3+},Sm^{3+} phosphor. J. Lumin. 243.

Cao, R., Zheng, Y., Cheng, T., Lan, B., Li, L., Zhng, Q., Nie, S., Wang, J., 2022b. Synthesis and tunable emission from yellow-green to red-orange of $Ca_3MgSi_2O_8$:Eu^{3+},Dy^{3+} phosphor. J.mol.Struct. 1262.

Chemingui, S., Ferhi, M., Horchani-Naifer, K., Ferid, M., 2015. Synthesis and luminescence characteristics of Dy^{3+} doped $KLa(PO_3)_4$. J. Lumin. 166, 82–87.

Chen, Y., Ding, W., Li, P., Li, X., Ba, Q., Liu, J., Qiu, K., Meng, X., Yang, Z., Wang, Z., 2019. A single-phase white light emitting phosphor $Ba_3Y(PO_4)_3$:Ce^{3+}/Tb^{3+}/Mn^{2+}: luminescence, energy transfer and thermal stability. RSC Adv. 9, 30406–30418.

Fu, X., Zheng, S., Shi, J., Liu, Y., Xu, X., 2018. Investigation of the cyan phosphor $Ba_2Zr_2Si_3O_{12}$:Eu^{2+},Dy^{3+} : mechanoluminescence properties and mechanism. J. Alloys Compd. 766, 221–228.

Gao, H., Li, P., 2018. Luminescence and energy transfer of white emitting phosphor $Ba_3Ce(PO_4)_3$:Dy^{3+}. Optik 170, 272–277.
Hu, J., Huang, T.H., Zhang, Y.P., Lu, B., Ye, H.Q., Chen, B.J., Xia, H.P., Ji, C.Y., 2019. Enhanced deep-red emission from Mn^{4+}/Mg^{2+} co-doped $CaGdAlO_4$ phosphors for plant cultivation. Dalton Trans. 48, 2455–2466.
Hunter, P.G., Spooner, A., Smith, B.W., Creighton, D.F., 2012. Investigation of emission spectra, dose response and stability of luminescence from NaCl. Radiat. Meas. 47, 820–824.
Jamalaiah, C., Jayasimhadri, M., 2019. Tunable luminescence properties of $SrAl_2O_4$:Eu^{3+} phosphor for LED applications. J. Mol. Struct. 1178, 394–400.
Kher, R.S., Panigrahi, A.K., Dhoble, S.J., Khokhar, M.S.K., 2006. Correlation between thermoluminescence and mechanoluminescence of gamma-irradiated Dy activated potassium and magnesium mixed sulphate. Radiat.Prot.Dosim. 119, 66–70.
Klym, Halyna, Karbovnyk, I., Luchechko, A., Kostiv, Y., Pankratova, V., Popov, A.I., 2021. Evolution of free volumes in polycrystalline $Baga_2O_4$ ceramics doped with Eu^{3+} ion. Crystals 11, 1515.
Lakshmanan, A.R., Jose, M.T., Annalakshmi, O., 2008. High-Sensitive $CaSO_4$:Dy thermoluminescent phosphor synthesis by co-precipitation Technique. Radiat.Prot. Dosim. 132, 42–50.
Lee, S.H., Won, Y.H., Jeon, D.Y., 2009. Improvement of electroluminescent properties of blue LED coated with highly luminescent yellow-emitting phosphors. Appl. Phys. B 95, 715–720.
Li, Chao, Zheng, H.W., Wei, H.W., Qiu, S.J., Xu, L., Wang, X.M., Jiao, H., 2018. Color tunable and white light emitting $Ca_2Si_5N_8$:Ce^{3+}, Eu^{2+} phosphor via efficient energy transfer for near-UV white LEDs. Dalton Trans. 47, 6860–6867.
Liu, H., Yu, L., Li, F., 2012. Photoluminescent properties of Eu^{3+} and Dy^{3+}ions doped $MgGa_2O_4$phosphors. J. Phys Chem solids. 74, 196–199.
Liu, S., Ma, S., Wang, S., Ye, Z., 2019. Exploring crystal-field splitting of Eu^{3+} ions in γ –and β-$SrGa_2O_4$. J. Lumin. 210, 155–163.
Manam, J., Das, S., 2010. Characterization and TSL dosimetric properties of Mn doped $BaSO_4$ phosphor prepared by recrystallisation method. J. Alloys Compd. 489, 84–90.
Matsui, H., Xu, C.-N., Akiyama, M., Watanabe, T., 2000. Strong mechanoluminescence from UV-irradiated spinels of $ZnGa_2O_4$:Mn and $MgGa_2O_4$:Mn. Jpn. J. Appl. Phys. 39, 6582–6586.
McCamy, C.S., 1992. Correlated color temperature as an explicit function of chromaticity coordinates. Color Res. Appl. 17, 142–144.
Mlotswa, D.V., Noto, L.L., Mofokeng, S.J., Obodo, K.O., Orante-Brron, Mothudi, B.M., 2020. Luminescence dynamics of $MgGa_2O_4$ prepared by solution combustion synthesis. Opt. Mater. 109.
Noto, L.L., Pitale, S.S., Gusowki, M.A., Ntwaeaborwa, O.M., Terblan, J.J., Swart, H.C., 2014. Luminescent dynamics of Pr^{3+} in $MTaO_4$ hosts (M=Y,La or Gd). J. Lumin. 145, 907–913.
Noto, L.L., Poelman, D., Orante-Barron, V.R., Swart, H.C., Mathevula, L.E., Chithambo, M., Mothudi, B.M., Dhlamini, M.S., 2017. Photoluminescence and thermoluminescence properties of $Baga_2O_4$. Physica B:Phys.Condens.Matter. 535, 268–271.
Pateria, Deepthi, Baghel, R.N., Bisen, D.P., 2015. Mechanoluminescence of Zns(1-x)(MnTe)x nanophosphors excited by impact load. J. Lumin. 166, 335–345.
Pathak, P.K., Kurchania, R., 2015. Synthesis and thermoluminescence properties of $SrAl_2O_4$ (Eu) phosphor irradiated with cobalt-60,6MV and 16MV photon beams. Rad.PhysChem. 117, 48–53.
Pathak, P.K., Kurchania, R., 2016. Thermoluminescence and kinetic parameters of synthesized $BaAl_2O_4$(Dy) phosphor irradiated with gamma and mega-voltage radiation. Optik 127, 1272–1276.
Poort, S.H.M., Blok poel, W.P., Blasse, G., 1995. Luminescence of Eu^{2+} in barium and strontium aluminate and gallate. Chem. Mater. 7, 1547–1551.
Praveena, R., Balasubrahmanyam, K., Jyothi, L., Venkataiah, G., Basavapoornima, C.H., Jayasankar, C.K., 2016. White light generation from Dy^{3+}-doped yitrium aluminium gallium mixed garnet nano-powders. J. Lumin. 170, 262–270.
Premkumar, H.B., Sunitha, D.V., Nagabhushna, H., Sharma, S.C., Nagabhushana, B.M., Shivakumara, C., Rao, J.L., Chakradhar, R.P.S., 2013. Synthesis, characterization, EPR, photo and thermoluminescence properties of $YAlO_3$:Ni^{2+} nanophosphors. J. Lumin. 135, 105–112.
Qiao, J.W., Zhao, Z., Liu, L., Xia, Z.G., 2019. Recent advances in solid-state LED phosphors with thermally stable luminescence. J. Rare Earths 37, 565–572.
Ryu, Hojin, Park, H.D., 1997. Photoluminescence properties of zinc gallate doped with Tm,Ce,Dy and Mn. J.Ind.Eng.chem. 3, 177–181.
Sharma, G., Lochab, Singh, S.P., 2010. TL behavior of $Ca_{0.5}Sr_{0.5}S$:Ce nano phosphors. J. Alloys Compd. 508, 9–12.
Shrivastava, R., Kaur, J., 2015. Chracterisation and mechanoluminescence studies of $Sr_2MgSi_2O_7$:Eu^{2+},Dy^{3+}. J.Rad.Res.Appl.Sc. 8, 201–207.
Sun, X.Y., Huang, S.m., Gong, X.S., Gao, Q.C., Ye, Z.P., Cao, C.Y., 2010. Spectroscopic properties and stimulation of white-light in Dy3+ doped silicate glass. J. Non-Cryst. Solids 356, 98–101.
Tangoulis, V., Lalioti, N., Parthenios, J., Boukos, N., Malina, O., Tucek, J.R., Zboril, J., 2018. Noncovalent grafting of a Dy_2^{III} single-molecule magnet onto chemically modified multiwalled carbon nantubes. Inorg. Chem. 57, 6391–6400.
Vijayakumar, R., Guo, H., Huang, X., 2018. Energy transfer and color-tunable luminescence properties of Dy^{3+}band Eu^{3+} co-doped $Na_3Sc_2(PO_4)_3$ phosphors for near-UV LED-based warm white LEDs. Dyes Pigments 156, 8–16.
Wei, Mi, Luan, C., Li, Z., Zhao, C., Feng, X., Ma, J., 2013. Ultraviolet-green photoluminescence of β-Ga2O3 films deposited on $MgAl_6O_{10}$(100) substrate. Opt. Mater. 35, 2624–2628.
Xiong, F.B., Liu, S.X., Lin, H.F., Meng, X.G., Lian, S.Y., Zhu, W.Z., 2018. A novel white-light-emission phosphor Dy^{3+}-doped $CaLaB_7O_{13}$ under UV excitation. Opt Laser. Technol. 106, 29–33.
Xuanhu, C., Jagadish, Chennupati, Ye, Jiandong, 2021. Fundamental properties and power electronic device progress of gallium oxide. Oxide Electronics 235–352.
Yu, M., Zhang, W., Yan, G., Dai, S., Qiu, Z., Zhang, L., 2018. Warm White emission property of $CaSr(PO_4)_2$:Dy^{3+} phosphors with red compensation by Eu^{3+} co-doping. Ceram. Int. 44.
Zhang, J.C., Xu, C.N., Long, Y.Z., 2013. Elastico-mechanoluminescence in $CaZr(PO_4)_2$: Eu^{2+} with multiple trap levels. Opt Express 21, 13699–13709.
Zhao, J., Zhang, W., Xie, E., Ma, Z., Zhao, A., Liu, Z., 2011. Structure and Photoluminescence of β-Ga_2O_3:Eu^{3+} nano fibers prepared by electro spinning. Appl. Surf. Sci. 257, 4968–4972.
Zhao, J., Sun, X., Wang, Z., 2018. Ce^{3+}/Eu^{2+} doped $SrSc_2O_4$ phosphors: synthesis, luminescence and energy transfer from Ce^{3+} to Eu^{2+}. Chem. Phys. Lett. 691, 68–72.
Zhao, M., Liao, H., Molokeev, M.S., Zhou, Y., Zhang, Q., Liu, Q., Xia, Z., 2019. Emerging ultra-narrow-band cyan-emitting phosphor for white LEDs with enhanced color rendition. Light Sci. Appl. 38.
Zhuang, Y., Xie, R-j., 2021. Mechanoluminescence rebrightening the process of stress sensing:A review. Adv.Materials. 33.